Kolmogorov-Johnson-Mehl-Avrami kinetics in different metrics

A. Korobov*
Materials Chemistry Department, V. N. Karazin Kharkov National University, Kharkov 61077, Ukraine
(Received 14 September 2006; revised manuscript received 15 May 2007; published 23 August 2007)

Two-dimensional random Voronoi tessellations with three different metrics are compared in terms of the Kolmogorov-Johnson-Mehl-Avrami approach. The main reason for this is to take into account the lattice symmetry in describing the kinetics of birth-growth processes at single crystal faces. Metrics of discrete random tessellations originating in this context and their continual analogs are determined by the unrestricted (prior to the first impingement) growth of a nucleus and differ from the Euclidean one. The free boundary length as a function of the nucleus radius is shown to be sensitive to the metric.

DOI: 10.1103/PhysRevB.76.085430 PACS number(s): 68.55.Ac, 05.20.Dd, 81.15.Aa

I. INTRODUCTION

The use of random tessellations in describing various birth-growth processes is partly rooted in Ref. 1. Together with Refs. 2 and 3, it originated the well-known Kolmogorov-Johnson-Mehl-Avrami (KJMA) approach. Originally developed for simulating the kinetics of steel crystallization, this approach was later extended to the fields of solid state reaction kinetics[4] and thin film growth.[5] A random tessellation is the direct ultimate result of a nucleation and growth to impingement process. In the extreme case of simultaneous nucleation and linear growth, it is termed the random Voronoi tessellation; a two-dimensional (2D) example is shown in Fig. 1. To get analytical relationships, the problem is reformulated in terms of coverings, as illustrated in Fig. 2. For the totality of circles, it is easy to calculate extended quantities, total area, and perimeter length. The theory gives the following relationship between actual and extended conversions:

$$\alpha = 1 - \exp(-\alpha_{ext}). \tag{1}$$

The applicability of the KJMA approach is restricted by the following conditions:[2] (i) nuclei are small compared to the reaction space, (ii) nucleation is according to Poisson, (iii) all nuclei have the same convex shape and orientation, and (iv) the growth law is the same for all the nuclei. Obviously, the reality is much richer. A large amount of work has been done to pass these limits, both in terms of coverings and tessellations. The progress is especially notable in the field of thin film growth. This includes, in particular, the account of the correlated nucleation,[6–9] the concepts of capture zones and scaling properties,[10–14] the simulation of highly anisotropic growth.[15,16]

One more interesting step to be made is to take the symmetry of a substrate into account. The use of the KJMA approach in its conventional form implies the Euclidean metric. In particular, Figs. 1 and 2 correspond to the Euclidean plane. Generally, the influence of substrates is diverse and difficult to register. If the growth process is linked to the (translational) symmetry of a substrate, the metric is different. To study this effect *per se* and to make use of the possible analytical calculations, the extreme model case of the simultaneous nucleation and the same growth law for all the nuclei is considered. Approaches in terms of coverings and tessellations are complementary. The former provides simple analytical formulas, whereas the latter is capable of a keener insight into geometrical details of a birth-growth process. This will be used below to compare different metrics determined by different crystal faces.

II. CRYSTAL FACE: MAIN TYPES OF DISCRETE RANDOM TESSELLATIONS

Any single crystal face is characterized by definite symmetry and combinatorial-topological structure. Its translational symmetry is described in terms of the Wigner-Seitz cells. Two distinctions from the Euclidean plane, the discreteness and metric, are essential in the present context. The former is determined by the parameters of the crystal lattice, and the latter by the mode of unrestricted (prior to the first impingement) growth of a nucleus.

The simplest situation corresponds to two following assumptions: a seed nucleus has the shape of the Wigner-Seitz cell of a substrate; and during the growth process, the interface propagates simultaneously to all adjacent symmetrically equivalent cells. At first glance, the former seems quite unrealistic. A seed nucleus is formed at random, and generally different nuclei may have different shapes as well as different numbers of atoms. However, if the influence of a substrate is significant, these different random nuclei may assume with time the same form determined by the symmetry. This point is discussed in detail in Ref. 17. It is logical to start with nuclei the symmetry of which corresponds to that of a substrate. The Wigner-Seitz cell as a seed nucleus is a reasonable model easily extendable to more realistic cases.

2D Wigner-Seitz cells may be either quadrangles or hexagons. Accordingly, we will be interested in random discrete

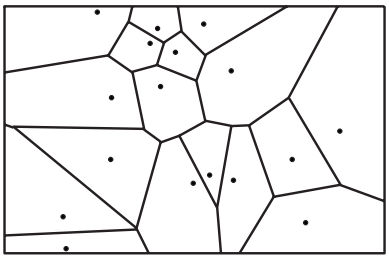

FIG. 1. Random Voronoi tessellation in the Euclidean metric.

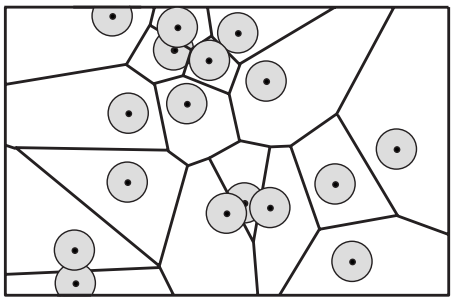

FIG. 2. Random covering compared to random tessellation; the set of nuclei is the same as in Fig. 1.

tessellations on quadrangle or hexagonal grids. The hexagonal grid is sketched in Fig. 3, which illustrates how the unrestricted growth of a nucleus determines the corresponding metric. The distance between any two nuclei (solid hexagons) is measured as the number of hexagons in the shortest chain between them (solid lines). With respect to the central nucleus, the whole grid is subdivided into two parts, A and B in Fig. 3. In region A and centrally symmetrical region, the distance is determined by the relationship $\mathrm{dist}_H=|\Delta x|+|\Delta y|[(1-\cos\psi)/\sin\psi]$, where ψ is the translational angle. In the case of regular hexagons, $\psi=60°$, but generally, ψ may be different. The subscript H denotes the hexagonal metric (H metric). In region B, the distance is $\mathrm{dist}_H=\Delta y/\sin\psi$. On the whole, the H metric is defined as follows:

$$\mathrm{dist}_H=\begin{cases}|\Delta x|+|\Delta y|\dfrac{1-\cos\psi}{\sin\psi}, & \dfrac{|\Delta y|}{|\Delta x|}<\tan\psi\\[2ex] \dfrac{|\Delta y|}{\sin\psi}, & \dfrac{|\Delta y|}{|\Delta x|}\geqslant\tan\psi.\end{cases}\tag{2}$$

The circle in this metric is the regular hexagon oriented as shown in the right bottom corner of Fig. 3. For the quadrangle lattice (Fig. 4), $\psi=90°$ and the corresponding metric (Q metric) is defined as

$$\mathrm{dist}_Q=|\Delta x|+|\Delta y|.\tag{3}$$

The Euclidean metric will be termed the E metric.

III. UNIFORM DISCRETE RANDOM TESSELLATIONS

In studying discrete random tessellations, one faces a number of peculiarities that have no analogs in conventional continual cases. In particular, this concerns domain boundaries.

In the conventional case shown in Fig. 1, boundaries of domains have fairly simple structure. They are lines each point of which is equidistant from two nuclei except vertices that are equidistant from three nuclei. Boundaries of discrete tessellations are more involved. Figure 4 illustrates this in the case of the square grid. The boundary is a line only if the distance between nuclei is odd (nuclei a and b in Fig. 4). If the distance is even (nuclei b and c), the boundary consists of cells. Linear boundaries look simpler, but this impression is wrong. Part of a linear boundary may be equidistant from two nuclei whereas another part is equidistant from three or more nuclei, and it is not a simple task to distinguish these parts in numerical computations.

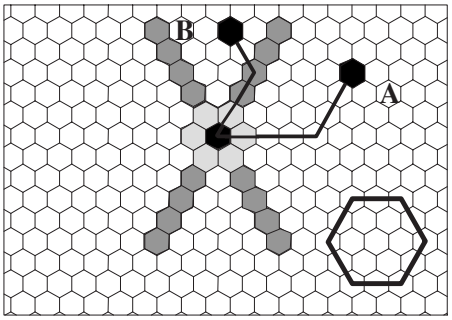

FIG. 3. The growth of a nucleus on the hexagonal grid; the boundary propagates simultaneously from a seed nucleus (solid hexagon) to all adjacent symmetrically equivalent cells (light gray filling).

If no restrictions are posed on the positions of nuclei, the corresponding tessellation will have mixed boundaries (right part of Fig. 4). It is impossible to construct tessellations with only linear boundaries. However, it is possible to construct tessellations with only cellular boundaries: the square grid is considered as a big chessboard and nuclei are placed at random on either black or white cells. Only this type of discrete random tessellations will be considered here. Tessellations of this type will be termed uniform tessellations.

In this case, the boundary between two nuclei has the following structure (see Fig. 4):

(1) The number of cells in its stepwise part is equal to $\min(|\Delta x|,|\Delta y|)+1$.

(2) If the origin of coordinates is associated with one of the nuclei (e.g., nucleus b in Fig. 4), one of these cells is surely situated on one of the axes.

(3) The stepwise part may be prolonged (*ad infinitum* if only two nuclei are considered) in both directions by straight parts oriented along the second axis.

(4) The stepwise part may consist of only one cell; in this case, one gets simply a straight boundary parallel to one of the axes.

IV. COMPARISON OF TESSELLATIONS WITH DIFFERENT METRICS

There is no natural discretization for conventional Euclidean tessellations. Accordingly, the only way to compare the

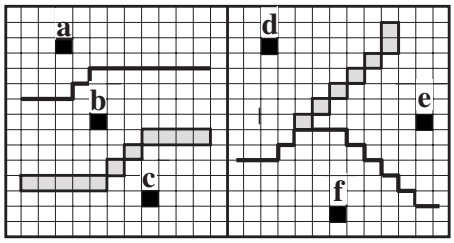

FIG. 4. Two different types of boundaries on the square grid; the type is determined by the distance between corresponding nuclei.

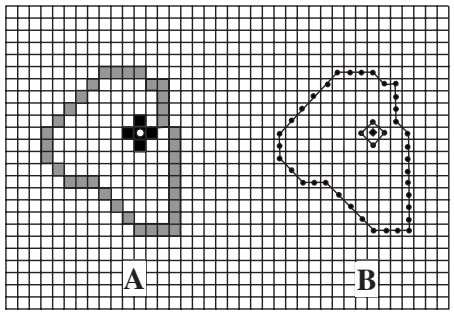

FIG. 5. Transition from a discrete model A to its continual analog B.

above discrete tessellations with the Euclidean one is to construct continual analogs for the former.

Figure 5 illustrates the approach in the case of the Q metric. One of the main parameters of continual tessellations is the density λ, which is the number of nuclei per unit area. In the discrete case, a nucleus itself has a definite area, and the density Λ is the ratio of the number of nuclei to the total number of grid cells. If the area of the cell is σ, then $\lambda = \Lambda/\sigma$. The perimeter length of a growing nucleus is counted in the discrete case as the number of cells forming its boundary. Thus, defined perimeter length is independent of the discreteness parameters. To pass to the continual analog, one needs to join centers of corresponding cells (Fig. 5). Perimeter lengths of the discrete nucleus A in Fig. 5 and its continual analog B expressed as the number of cells are the same. If the cell edge equals a, the distance between the centers of adjacent cells is $2a$ (Q metric). The boundary of a nucleus is uninterrupted only until its first impingement with the boundary of the corresponding domain of the tessellation. The number of boundary cells η and the number of linking pieces χ are equal. The first impingement results in the break of the boundary, and $\chi = \eta - 1$. Generally, the boundary of a nucleus has z breaks and its size l in units of length is related to that counted as the number of cells η by the linear relationship

$$l = 2a(\eta - z). \tag{4}$$

In the discrete case, the nucleus radius is naturally expressed as the step number s: at each step, the boundary propagates to all adjacent symmetrically equivalent cells. The same increment may be chosen for convenience in the continual case. Two continual random tessellations resulting from the same set of nuclei as in Fig. 1, but corresponding to metrics Q and H, are shown in Figs. 6 and 7, respectively.

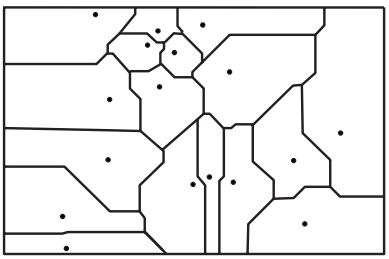

FIG. 6. Random Voronoi tessellation in the Q metric; the set of nuclei is the same as in Fig. 1.

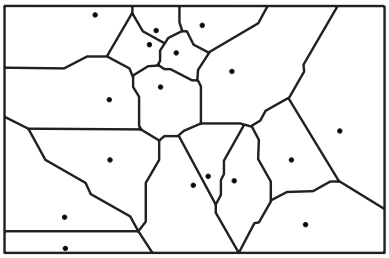

FIG. 7. Random Voronoi tessellation in the H metric; the set of nuclei is the same as in Fig. 1.

Figure 8 illustrates the way in which kinetic properties of tessellations were compared numerically. Each domain of a random tessellation is considered as a "rightful domain" of a growing nucleus, and the growth of this nucleus is followed from the very beginning by plotting the free boundary length (with the account of impingements) on radius. An example obtained as the direct computer output for one cell is shown in Fig. 9. Each peak of this curve corresponds to the impingement of a nucleus with one of the domain edges, which simulates impingements of nuclei. This dependence $l(r)$ for a single nucleus is termed the primitive kinematic curve. The term "kinematic" is used to emphasize that no reference is made to actual driven forces of a birth-growth process. The resulting curve $L(r)$ is the sum of all primitive curves of the tessellation averaged over the nucleus population.

Kinematic curves $L(r)$ of all three tessellations have been computed in the following way:

(1) 10 000 nuclei were placed at random on a plane to provide the density $\lambda = 1$.

(2) Tree primitive curves $l_E(r)$, $l_Q(r)$, and $l_H(r)$ were calculated for each nucleus. To do this, the nucleus radius r was varied in the range $[0, r_{\text{final}}]$ with the step 0.01; r_{final} was determined by the conditions $l_E(r_{\text{final}}) = 0$, $l_Q(r_{\text{final}}) = 0$, and $l_H(r_{\text{final}}) = 0$. At each step, the part of the nucleus boundary which is closer to its nucleus than to any other nucleus was identified in each metric. Generally, the length of this part of

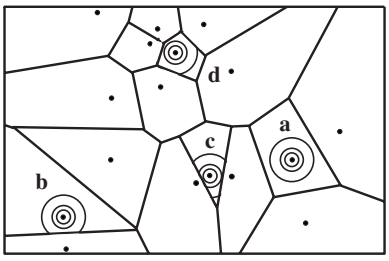

FIG. 8. A kinetic view of the random Voronoi tessellation. The set of nuclei is the same as in Fig. 1, but the growth of only four nuclei is sketched for clarity. At a given value of the radius, the number of impingements is different for different nuclei: (a) no impingements; (b) one impingement, the boundary is singly connected; (c) two impingements, the boundary is doubly connected; and (d) four impingements, the boundary is singly connected.

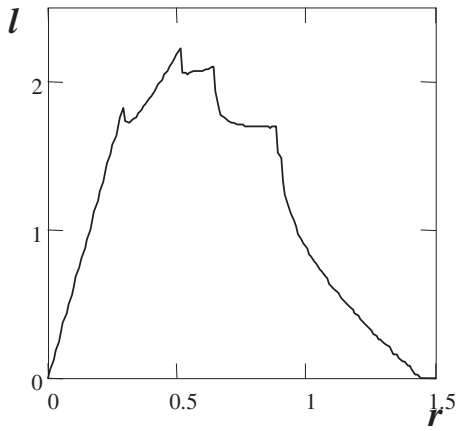

FIG. 9. An example of the primitive kinematic curve; four peaks correspond to four successive impingements of a growing nucleus with boundaries of its four-edge domain.

the boundary may be calculated in two ways: in one and the same Euclidean metric for all three mosaics and for each mosaic in its metric. The former approach is used in the present paper.

(3) Thus, the obtained primitive curves were then summed up over all domains and divided by the total number of nuclei.

In the simplest case of Voronoi tessellations, the same quantities may be calculated analytically exploiting the idea of extended quantities.[1] The extended boundary length and extended conversion are as follows:

$$L_{ext}(r) = \begin{cases} 2\pi r\lambda \\ 4\sqrt{2}r\lambda \\ 6r\lambda, \end{cases} \qquad \alpha_{ext} = \begin{cases} \pi r^2\lambda & (E \text{ mosaic}) \\ 2r^2\lambda & (Q \text{ mosaic}) \\ \dfrac{3\sqrt{3}}{2}r^2\lambda & (H \text{ mosaic}). \end{cases} \tag{5}$$

The actual free boundary length $L(r)$ is equal to $(1-\alpha)L_{\text{ext}}(r)$, where α is given by Eq. (1). Accordingly,

$$L(r) = \begin{cases} 2\pi r\lambda \exp(-\pi r^2\lambda) & (E \text{ mosaic}) \\ 4\sqrt{2}r\lambda \exp(-2r^2\lambda) & (Q \text{ mosaic}) \\ 6r\lambda \exp\left(-\dfrac{3\sqrt{3}}{2}r^2\lambda\right) & (H \text{ mosaic}). \end{cases} \tag{6}$$

$L(r)$ curves computed both analytically and numerically for three different metrics are compared in Fig. 10. Obviously, they represent different kinetics. The agreement of analytical and numerical results is reasonably good.

With the boundary length calculated for comparison in the same Euclidean metric for all three mosaics, as described above, values of $S=\int_0^\infty L(r)dr$ are as follows: $S_E=1$, $S_Q=\sqrt{2}$ (1.414), and $S_H=2/\sqrt{3}$ (1.155), and $\lambda=1$. The same ratio of areas may be obtained as shown in Fig. 11. A nucleus is placed in the center of a unit square, and its growth is followed in three metrics until the square is completely covered by the nucleus. The free boundary length may be expressed as the function of radius analytically:

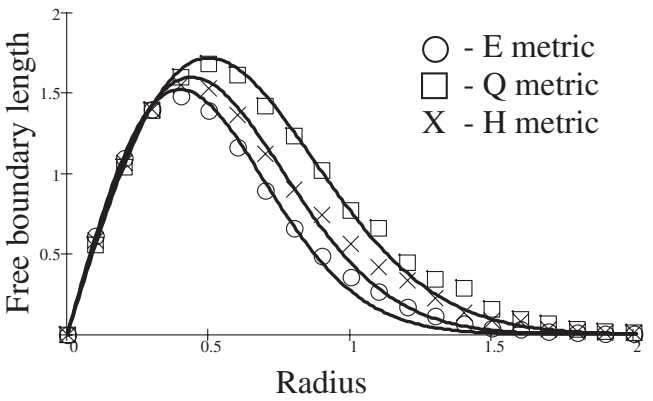

FIG. 10. Kinematic curves for the same set of nuclei calculated analytically (solid lines) and numerically (symbols) for three different mosaics in the Euclidean metric.

$$l_E(r) = \begin{cases} 2\pi r, & 0 \leqslant r \leqslant \dfrac{1}{2} \\ 4r\left(\dfrac{\pi}{2} - 2\arcsin\sqrt{1-\dfrac{1}{4r^2}}\right), & \dfrac{1}{2} \leqslant r \leqslant \dfrac{1}{\sqrt{2}}, \end{cases} \tag{7}$$

$$l_Q(r) = \begin{cases} 4\sqrt{2}r, & 0 \leqslant r \leqslant \dfrac{1}{2} \\ 4\sqrt{2}(1-r), & \dfrac{1}{2} \leqslant r \leqslant 1, \end{cases} \tag{8}$$

$$l_H(r) = \begin{cases} 6r, & 0 \leqslant r \leqslant \dfrac{1}{2} \\ 4-2r, & \dfrac{1}{2} \leqslant r \leqslant \dfrac{1}{\sqrt{3}} \\ 4\left(1+\dfrac{1}{\sqrt{3}}-2r\right), & \dfrac{1}{\sqrt{3}} < r \leqslant \dfrac{1}{2}+\dfrac{1}{2\sqrt{3}}. \end{cases} \tag{9}$$

The areas under these curves are $s_E=1$, $s_Q=1.414$, and $s_H=1.155$.

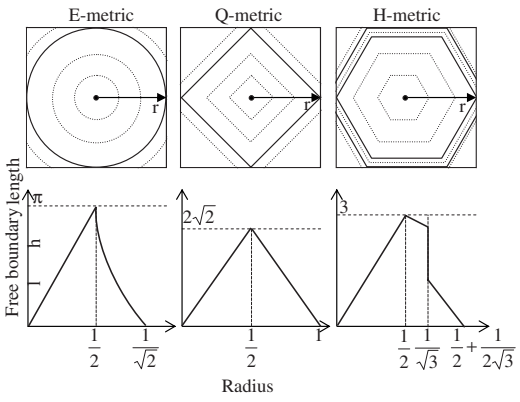

FIG. 11. Primitive kinematic curves for a nucleus in the center of a unit square.

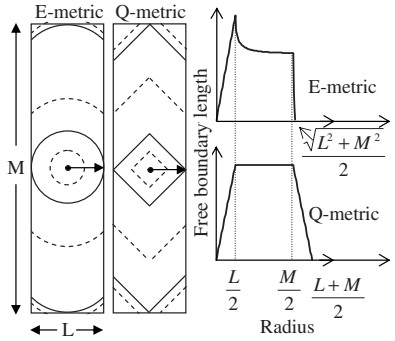

FIG. 12. Primitive kinematic curves for a nucleus in the center of a unit domain ($L\times M=1$).

The shape of the unit domain may be changed, but the discussed ratio of areas remains invariant. An example is given in Fig. 12. Equations for the free boundary length are as follows:

$$l_E(r)=\begin{cases} 2\pi r, & 0\leqslant r\leqslant \dfrac{L}{2} \\ 2r\left(\pi-2\arccos\dfrac{L}{2r}\right), & \dfrac{L}{2}\leqslant r\leqslant \dfrac{M}{2} \\ 4r\left(\dfrac{\pi}{2}-\arccos\dfrac{L}{2r}-\arccos\dfrac{M}{2r}\right), & \dfrac{M}{2}\leqslant r\leqslant \dfrac{\sqrt{L^2+M^2}}{2}, \end{cases} \tag{10}$$

$$l_Q(r)=\begin{cases} 4\sqrt{2}r, & 0\leqslant r\leqslant \dfrac{L}{2} \\ 2\sqrt{2}L, & \dfrac{L}{2}\leqslant r\leqslant \dfrac{M}{2} \\ 4\sqrt{2}\left(\dfrac{L+M}{2}-r\right), & \dfrac{M}{2}\leqslant r\leqslant \dfrac{L+M}{2}. \end{cases} \tag{11}$$

The corresponding areas are $s_E=1$ and $s_Q=1.414$. For the H metric, the figure and formulas are somewhat cumbersome to be reproduced here but $s_H=1.155$. This provides an insight into the interrelation between the metric and the nucleus shape.

In the case of the E metric, the values of $r_{\max}$ were shown to be close to half of the averaged distance to the second nearest nucleus in the population.[18] This corresponds to the value of r for the highest peak (Fig. 9) averaged over all primitive curves (or, in other words, the distance to the second nearest edge averaged over the Voronoi tessellation). Distances δ_k to the nearest, second, etc., nuclei can be calculated analytically exploiting the known density function[19]

$$f(\delta_k)=2(\lambda\pi)^k[(k-1)!]^{-1}\exp(-\lambda\pi\delta_k^2)\delta_k^{2k-1}, \tag{12}$$

where k enumerates these neighbors. For averaged distances $\langle\delta_k\rangle$, it gives

$$\langle\delta_k\rangle=\frac{\Gamma(k+1/2)}{(k-1)!\sqrt{\pi\lambda}}, \tag{13}$$

where $\Gamma(x)$ is the Euler function. With this in mind, averaged distances to neighbors have been numerically computed for the above set of 10 000 nuclei with density $\lambda=1$ in three metrics. Results divided by 2 are given in Table I. According to Eq. (6), $r_{\max}$ is equal to $1/\sqrt{2\pi\lambda}$ for the E metric, $1/2\sqrt{\lambda}$ for the Q metric, and $1/\sqrt{3\sqrt{3}\lambda}$ for the H metric (numerical values for $\lambda=1$ are 0.399, 0.5, and 0.439, respectively).

One more point is to examine the area distribution functions of the Voronoi domains in three metrics. This has been done in the following way. First, 10 000 nuclei were placed at random within 100×100 square, providing $\lambda=1$. Then, 1 000 000 test points were placed at random within the same square. In each metric, each test point was attributed to the nearest nucleus. The percentage of test points belonging to a given nucleus determines the area of its domain (as a share in the total area). The result is 10 000 values of domain areas for each metric. Since $\lambda=1$, they are scaled as $S/\bar{S}$. Histograms constructed from these data were normalized to the unit area under them. Results are shown in Fig. 13. Surprisingly, there are no significant differences; area distributions are practically the same for all three metrics. The solid line in Fig. 13 corresponds to the commonly used Kiang conjecture[20]

$$F(y)=\frac{c^c}{\Gamma(c)}y^{c-1}\exp(-cy). \tag{14}$$

The parameter $c=3.63$ is in a reasonable agreement with that mentioned in the literature.[20–22]

This result for area distributions raises the question about the relationship of neighborhood for the same nuclei in different metrics. Figure 14 shows that the neighborhood is changed for some nuclei in passing from the E metric to Q

TABLE I. Averaged distances to neighbors (divided by 2) in three metrics for the same set of nuclei ($\lambda=1$).

	Neighbor						
Metric	1	2	3	4	5	6	7
E [Eq. (13)]	0.250	**0.375**	0.469	0.547	0.615	0.677	0.733
E	0.249	**0.375**	0.468	0.546	0.615	0.676	0.733
Q	0.313	**0.470**	0.587	0.684	0.770	0.847	0.918
H	0.274	**0.412**	0.514	0.601	0.676	0.744	0.806

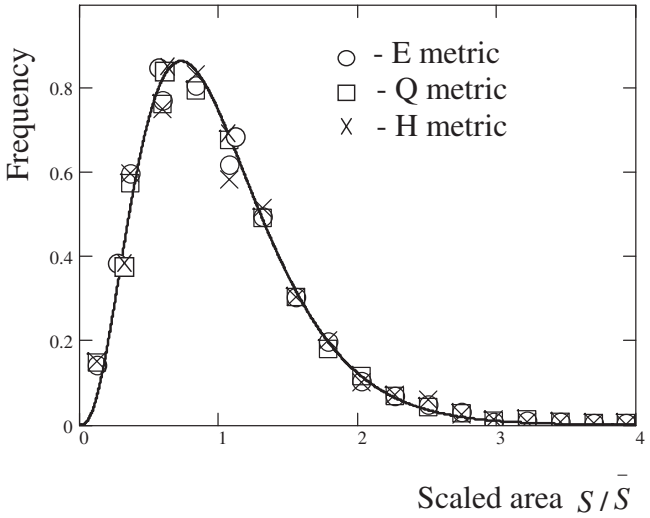

FIG. 13. Area distributions of domains in three metrics (symbols) in comparison with the Kiang conjecture (solid line).

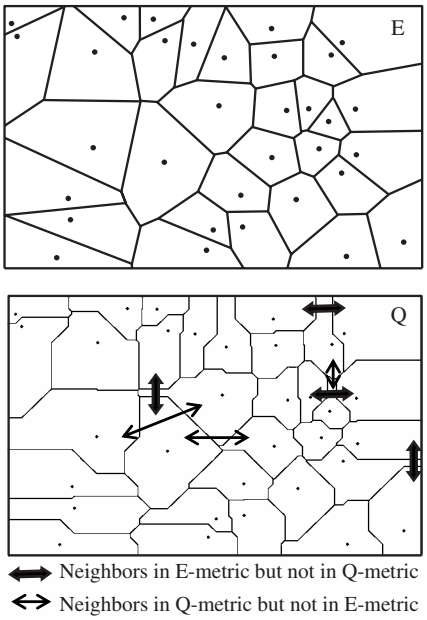

FIG. 14. The change of neighbors in passing from the E metric to Q metric.

metric. In this small fragment, four neighbors in the E metric are no longer neighbors in the Q metric; instead, three non-neighbors in the E metric are neighbors in the Q metric. In 30 similar small tessellations, the number of new neighbors and of new non-neighbors are approximately the same. This holds true in passing from the E metric to H metric. A detailed comparative statistics of the neighborhood is an involved problem which is beyond the scope of this paper.

V. SUMMARY

2D random Voronoi tessellations with three different metrics have been compared with respect to KJMA kinetics. The motivation for this study is to take the symmetry of the surface lattice into account in describing birth-growth processes which may be linked to this symmetry. Two metrics compared with the conventional Euclidean metric are determined by the two main types of 2D Wigner-Seits cells. The corresponding random Voronoi tessellations are discrete. Peculiarities of their boundaries are briefly discussed and continual analogs are constructed for comparison with the Euclidean metric. The present study is restricted to the simplest model: simultaneous nucleation and the same growth law for all the nuclei. This is warranted by analytical calculations possible in this case. The dependence of the free boundary length on radius is shown to be sensitive to the metric. Also, for some nuclei of the population, neighbors are changed with the change of metric. A surprising result is the invariance of the area distribution of Voronoi domains. Generally, the area is believed to be a more appropriate quantity for describing the kinetics of birth-growth processes. Here, we face the situation when the boundary length is a more sensitive characteristic. This argues in favor of complementarity of these two quantities in exploring various aspects of these many-sided processes. Where analytical calculations are possible, numerical results are in a reasonable agreement with them, which justifies the extension of the approach to more realistic but analytically intractable cases.

ACKNOWLEDGMENT

This research was partly supported by the Ukrainian Minister of Education and Science through Grant No. 0104U000663.

*alexander.i.korobov@univer.kharkov.ua

[1] W. A. Johnson and R. F. Mehl, Trans. Am. Inst. Min., Metall. Pet. Eng. **135**, 416 (1939).
[2] A. N. Kolmogorov, Bull. Acad. Sci. URSS **3**, 355 (1937); English translation: *Selected Works of A. N. Kolmogorov*, edited by A. N. Shiryayev (Kluwer, Dordrecht, 1992), Vol. 2, p. 188.
[3] M. Avrami, J. Chem. Phys. **7**, 1103 (1939); **8**, 212 (1940).
[4] M. E. Brown, D. Dollimore, and A. K. Galwey, *Reactions in the Solid State* (Elsevier, Amsterdam, 1980).
[5] M. Fanfoni and M. Tomellini, Nuovo Cimento Soc. Ital. Fis., D **20D**, 1171 (1998).
[6] M. Fanfoni and M. Tomellini, J. Phys.: Condens. Matter **17**, 571 (2005).
[7] M. Tomellini, M. Fanfoni, and M. Volpe, Phys. Rev. B **62**, 011300 (2000).
[8] M. Fanfoni, M. Tomellini, and M. Volpe, Phys. Rev. B **65**, 172301 (2002).
[9] M. Tomellini and M. Fanfoni, Phys. Rev. B **72**, 155407 (2005).
[10] P. A. Mulheran and J. A. Blackman, Philos. Mag. Lett. **72**, 55 (1995).

[11] P. A. Mulheran and J. A. Blackman, Phys. Rev. B **53**, 10261 (1996).
[12] P. A. Blackman and P. A. Mulheran, Comput. Phys. Commun. **137**, 195 (2001).
[13] D. M. Tarr and P. A. Mulheran, Phys. Rev. E **68**, 020602(R) (2003).
[14] M. C. Bartelt and J. W. Evans, Phys. Rev. B **54**, R17359 (1996).
[15] T. Pusztai and L. Gránásy, Phys. Rev. B **57**, 14110 (1998).
[16] B. J. Kooi, Phys. Rev. B **73**, 054103 (2006).
[17] A. Korobov, Complexity **4**, 31 (1999).
[18] A. Korobov, J. Math. Chem. **25**, 365 (1999).
[19] D. Stoyan, W. S. Kendall, and J. Mecke, *Stochastic Geometry and its Applications* (Wiley, Chichester, 1996).
[20] T. Kiang, Z. Astrophys. **64**, 443 (1966).
[21] D. L. Weaire, J. P. Kermode, and J. Wejchert, Philos. Mag. B **53**, L101 (1986).
[22] P. A. Mulheran, Philos. Mag. Lett. **66**, 219 (1992).